AIMS Energy, 12(2): 532–547.
DOI: 10.3934/energy.2024025
Received: 18 January 2024
Revised: 19 March 2024
Accepted: 29 March 2024
Published: 02 April 2024

http://www.aimspress.com/journal/energy

Research article

Indoor experiments of a horizontal multiple effects diffusion solar still: Influence of heat input and the number of stages

Abdulrahman Almutlaq*

Department of Mechanical Engineering, King Fahd University of Petroleum and Minerals, Dhahran 31261, Saudi Arabia

* **Correspondence:** Email: g202317190@kfupm.edu.sa; Tel: +966138600000.

Abstract: Clean water is important for human life, and obtaining it with the least amount of energy is significant. This research aims to desalinate water using a horizontal multiple effects diffusion solar still (DSS). A small distillation device with an area of 10 × 10 cm^2 was designed and 3D printed. An electric heater was used to simulate solar radiation at 400, 700, and 1000 W/m^2. The amount of water produced when using 1, 3, and 5 effects was recorded. The most notable results were: maximum water yield reached 1.93 kg/m^2 h at 1000 W/m^2, at which the solar to vapor conversion efficiency was 107%. The daily water yields throughout the year were estimated, and the maximum production was 10.16 kg/m^2 during a day in June, when the global horizontal irradiance was 7.01 kWh/m^2. The results were also compared with other distillation systems.

Keywords: solar energy; seawater; desalination; sustainability; solar still; wick

1. Introduction

One of the most important issues that directly affects human life is the lack of clean water. In 2019, it was reported that 1 in 3 people globally do not have access to safe drinking water [1]. Such a problem motivated researchers to develop different methods and technologies for water desalination, including thermal, membranes, and other advanced technologies [2]. This research focused on water distillation using thermal energy, due to its simple installation, low maintenance cost, and the abundance of solar energy that can be used for distillation [3]. However, solar stills have the disadvantage of low water output [4], so many researchers seek to create different designs for stills, such as pyramidal, spherical,

or double-slope, or add other elements to conventional stills, such as spraying nozzles [5], jute, mirrors, or phase change materials (PCM) [6]. Researchers are also trying to design hybrid distillation systems by adding a parabolic reflector for the purpose of increasing the concentration of solar radiation [7], adding a flat-plate collectors [8], or utilizing the waste heat of an electricity generator for the purpose of heating the seawater before it enters the solar still.

The multiple effects diffusion solar still is distinguished from the previous types in that it reutilizes the heat gained for evaporation in the first stage to evaporate another amount of water in subsequent stages, each consisting of an evaporator and a condenser. Due to this heat reutilization, an increase in the total water output occurs. This distiller can be in a vertical or horizontal position. The following subsection summarizes several studies of both vertical and horizontal distillers.

Fukuia et al. [9] studied horizontal diffusion solar still (DSS) coupled with long wicks. They absorb seawater to their evaporating zones by capillary force. The resulted vapor diffuses and condenses on facing wicks, which drives the water to storage bags. They noticed that evaporation rates from wicks decreased as the number of effects increased. They predicted water yield of 15 kg/m^2 day at 22 MJ/m^2 day for 6 effects. Tanaka [10] experimentally studied vertical 6-effects DSS with gap distance of 5 mm. The unit was coupled with a flat plate reflector. The maximum productivity reached 13.4 kg/m^2 day at average solar radiation of 21.55 MJ/m^2. Tanaka and Iishi [11] conducted an experimental study on vertical single-effect DSS coupled with a tilted wick still. The main objective of this design was to efficiently utilize the solar energy without using a sun tracker. The maximum water yield was 4.88 kg/m^2 day at 18.4 MJ/m^2 day on the still surface. Park et al. [12] experimentally studied hybrid solar still consisting of 11-effects DSS coupled with single slope basin type solar still. The seawater inside the basin was heated by solar energy as well as the rejected heat from an electricity generator by adding a heat exchanger inside the basin. The maximum water productivity was 18.02 kg/m^2 day at 22.37 MJ/m^2 day. Lim et al. [13] conducted a 2D numerical study to examine the performance of an 11-effects DSS. The gap distance was fixed at 5 mm. They found highest water yields of 7.32–7.80 kg/m^2 day during summer solstice. However, in spring/autumn equinoxes, the water yields were around 2.93–3.17 kg/m^2 day. The lowest water yield was in the winter where it dropped to 0.33–0.34 kg/m^2 day. Huang et al. [14] designed and implemented a novel 6-effects concentric configuration DSS with a thermal concentrator. The highest water yield was 2.2 kg/m^2 h at 1000 W/m^2 and three times the thermal concentration. Sharon et al. [15] conducted a numerical study on vertical DSS with a variable number of diffusion chambers ranged from 1 to 10 at variable solar intensities (100 to 1000) W/m^2. They showed that the three diffusion chambers configuration was cost effective. The annual average yield was 11.13 kg/m^2 day. Xu et al. [16] showed that vertical 10-effects DSS was able to reach a production rate of 5.78 L/m^2 h with well-insulated side walls and glass cover.

The aim of this research was to study horizontal DSS. Specifically, studying the effect of the heat input (400, 700, and 1000 W/m^2) and the number of stages (1, 3, and 5) on water yield.

2. Materials and methods

2.1. Working principle

The horizontal multiple effects solar still consists of several layers as in Figure 1. The first layer is a glass cover. It is originally used to transmit sunlight and reduce heat loss from the air below it. In this research, the experiments were not conducted under sunlight. Instead, an electric heating pad was

used to simulate sunlight. The second layer below the glass cover is the heating pad. A thermal conductor (aluminum sheet) is glued to the bottom of the thermal pad. Attached to the aluminum sheet is a wick. The sea water is continuously driven to the drier (less saturated) regions of the wicks by means of capillary action, as in Figure 1. When the temperature of the heating pad rises, the heat is transferred to the aluminum sheet (which acts as an evaporator) and then to the wick, whereby the seawater begins to evaporate. The water vapor travels over a distance to another wick located at the bottom and attached to another aluminum sheet (acting as a condenser). The heat of the water vapor is transferred to the condenser, so the water vapor condenses, and the wick absorbs this water and transfers it to the freshwater collection container, as in Figure 2. The heat gained by the condenser is either dissipated, and the device is then considered as "single effect", or it can be used again, by transferring the heat to another wick that is attached under the condenser and saturated with sea water. For this stage, the sheet is considered as an evaporator. The process of evaporation and condensation is repeated, in a manner similar to what was mentioned earlier. The device is then considered as "multiple stages" or "multiple effects" [9,17].

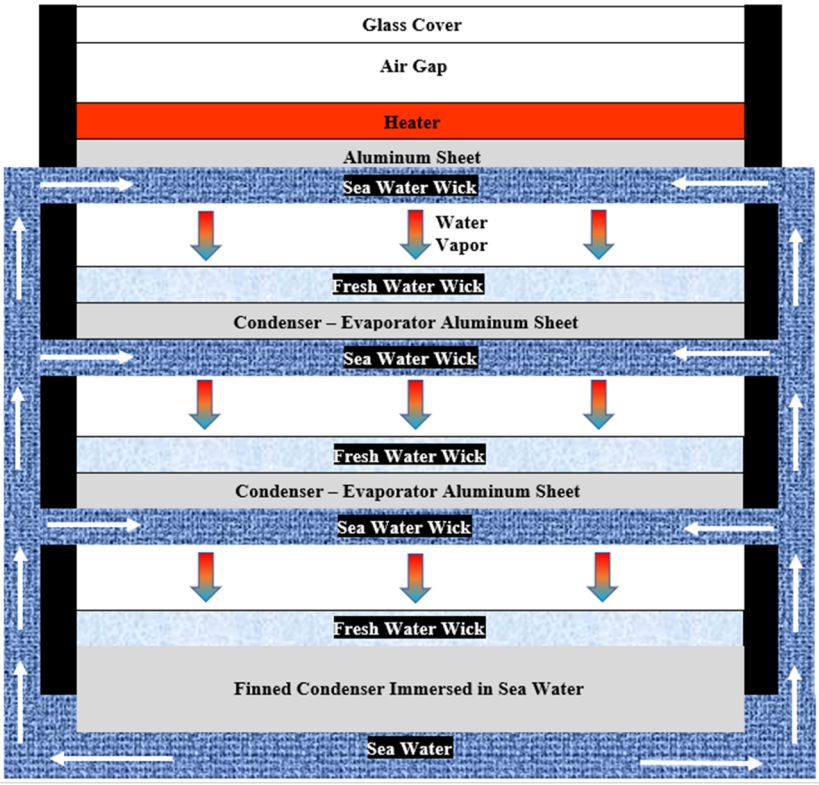

Figure 1. Side view of the horizontal 3 effects solar still.

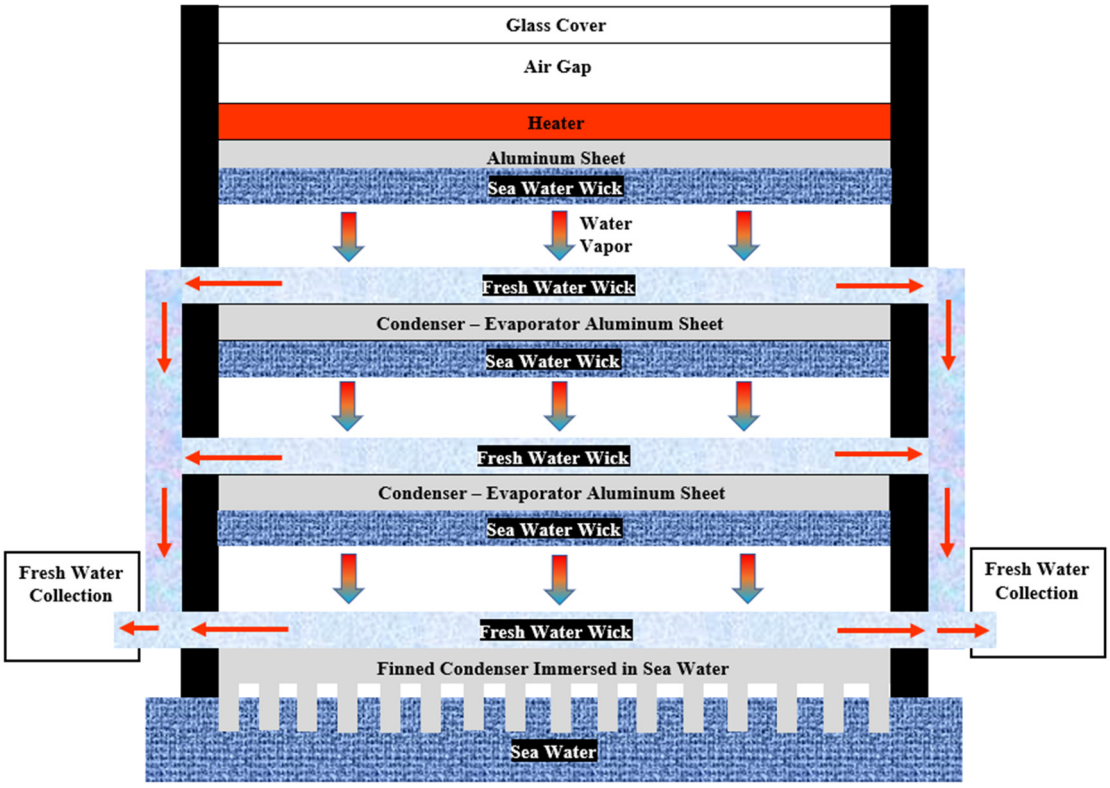

Figure 2. Front view of the horizontal 3 effects solar still.

2.2. Experiments apparatus

The distillation unit used in conducting the experiments consists of several parts, as shown in Figure 3. The parts shown in black were 3D printed out of PETG material with 25% infill. The upper cover was made of 4 mm-thick glass and had an area of (10 × 10) cm^2 (Figure 3a), and this area was fixed for all subsequent elements. The side wall thickness was 17 mm. Below the glass cover was the electric heating pad, which was 3 cm away (Figure 3b). A 0.5 mm-thick aluminum sheet was attached to the bottom of the heater. It was used as a heat conductor and evaporator for the seawater that collected in the wick at the bottom of the sheet. The used wick was a disposable towel (Cosma Belle) and was approximately 0.25 mm thick (Figure 3c). Directly under the wick was a two-post spacer (Figure 3d). The first function was to keep the seawater-saturated wick firmly attached to the aluminum sheet (evaporator) and prevent the middle of the wick from sagging downward. This was accomplished with a hexagonal mesh that held the wick and, at the same time, allowed the water vapor to pass through. The thickness of the mesh was 1 mm. The second function of the spacer was to maintain a distance of 6 mm between the seawater-saturated wick and the clean water wick. An aluminum sheet (Figure 3e) was located at the bottom of the wick collecting clean water (it was considered a condenser in this stage and an evaporator in the next stage) to which heat was transferred, causing the vapor to condense and be collected as clean water in a way that will be explained later. It should be noted that both types of wicks were wetted by deionized water before installation and were installed in perpendicular position as previously shown in Figures 1 and 2. Below the condenser-evaporator sheet, the following elements were repeated: seawater collecting wick-spacer-clean water collecting wick-condenser-evaporator sheet, and this assembly was considered as another stage/effect. At the end of the stages, a finned

condenser was installed (Figure 3f) with a base thickness of 4 mm and a fin length of 26 mm. Most of these fins were immersed in seawater for the purpose of enhancing heat dissipation.

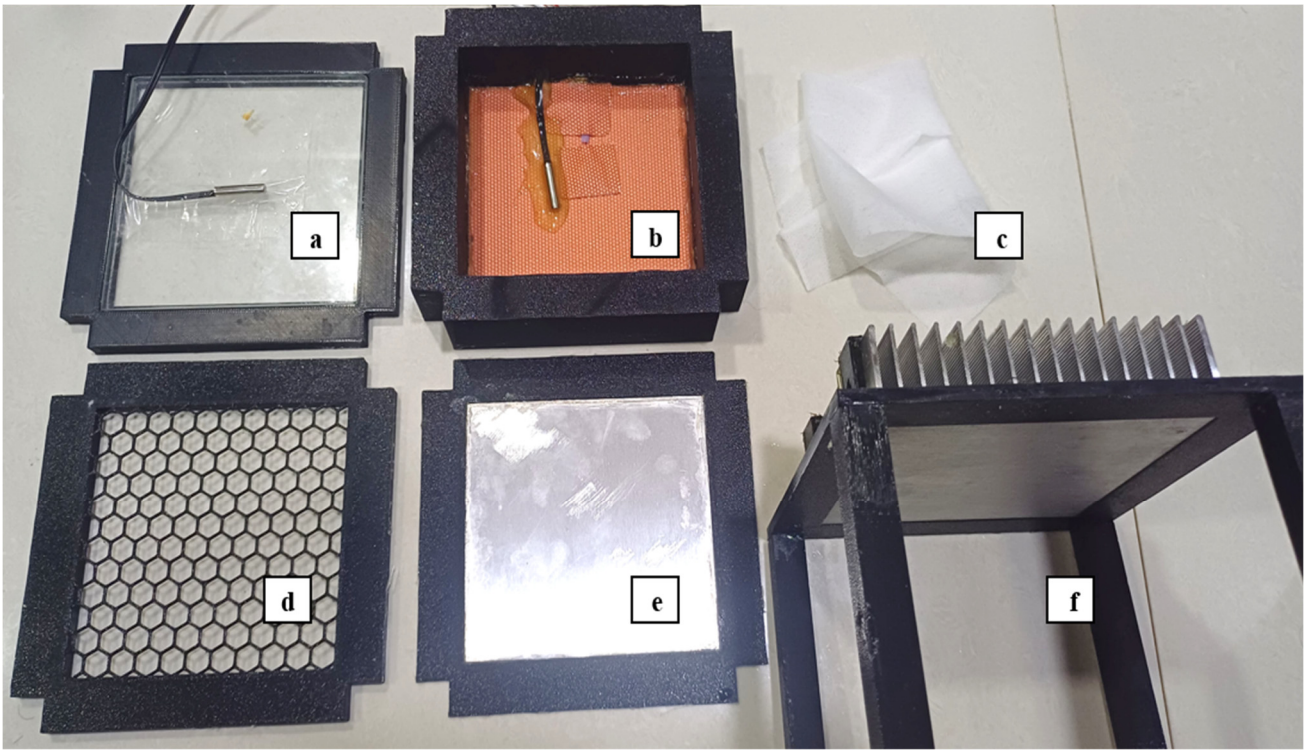

Figure 3. Photograph of disassembled horizontal multiple effects solar still: (a) glass cover; (b) pad heater; (c) disposable towel (repeated element); (d) spacer (repeated element) ; (e) condenser-evaporator sheet (repeated element); (f) last finned condenser.

Experiments were conducted as shown in Figure 4. A tub was filled with 30 liters of water and approximately 1 kg of salt was added, raising the total dissolved solids (TDS) to more than 33,000 ppm in order to simulate seawater (Figure 4f). The studied range of stages was 1, 3, and 5 effects. The distillation unit (Figure 4d) was assembled with a certain number of stages then positioned in a way that allowed the last finned condenser to be mostly immersed in water. Then the seawater-absorbing wick was dipped in water from both ends (one end is shown in Figure 4e, while the other end is not visible). The heat input of the electric pad heater was adjusted to a certain value with a power supply (Figure 4i). The studied range of the heat inputs was 400, 700, and 1000 W/m^2, and they were determined by Eq 1 [18].

$$q_{heater} = \frac{V\,I}{A} \tag{1}$$

where q_{heater} is the selected heat input, V is the voltage, I is the current, and A is the aperture area (10 × 10) cm^2. Both voltage and current were determined by trial and error, and it was noticed that they decreased as the temperature inside the unit increased, which required fine tuning of the DC power supply during the experiment until a steady state was reached ($dT/dt \approx 0$).

After the power supply was set to a certain value, the temperatures inside the system began to rise and were measured using five K-type thermocouple sensors. The measurements were shown in real

time on mini liquid crystal displays (Figure 4h). The temperature measurements included: glass surface from the outside T_g, the electric heating pad T_h, the last finned condenser T_c, the feed water T_w, and the ambient temperature T_{amb} (Figure 4g).

The wicks that collected water had two ends (one of them is labeled in Figure 4b). This end was placed between several layers of dry paper tissues that absorbs moisture, and was changed after reaching steady state. These tissues were placed in a plastic container whose weight was measured by a 0.1 g-accuracy weight scale before and after the experiment (Figure 4c), where the weight difference equaled the amount of clean water produced. The tissues were covered with a plastic cover to reduce evaporation of the collected water (Figure 4a).

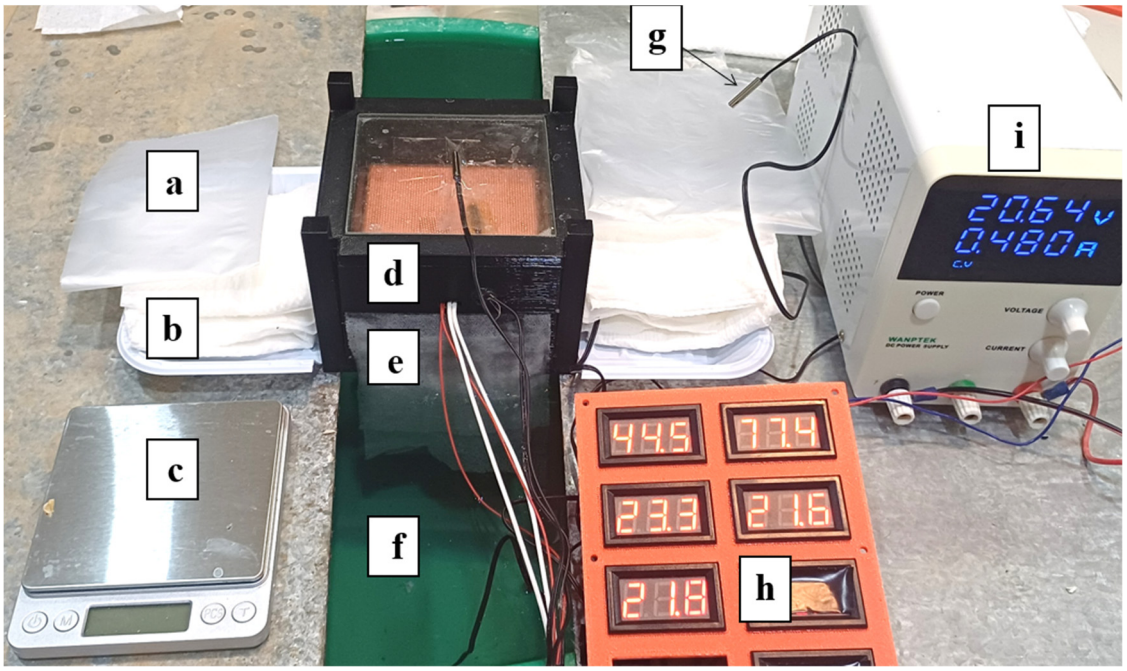

Figure 4. Experiment setup: (a) plastic cover; (b) fresh water collection; (c) weight scale; (d) horizontal multiple effects solar still; (e) sea water wicks; (f) sea water; (g) ambient temperature sensor; (h) temperature displays; (i) power supply.

Due to the small size of the distillation unit, the water yield from it during the experiment period was very small, and this caused difficulty in measuring the total dissolved solids (TDS). Therefore, after measuring the weight of the resulting water, which in the worst cases was not less than 2 g at 400 W/m^2 and with single effect configuration, deionized water was added to the resulted water, then both weight and TDS were measured. The initial TDS of the water was then calculated using Eq 2.

$$m_i \, TDS_i = m_f \, TDS_f \tag{2}$$

where m_i is the mass of water resulting from the distillation unit, TDS_i is the total dissolved solids of the resulted water from the distillation unit (to be calculated), m_f is the mass of resulted water plus the added deionized water, and TDS_f is the total dissolved solids of the resulted water plus the added deionized water.

2.3. Performance of horizontal multiple effects solar still

Many researchers agree on a method to calculate the solar to vapor conversion efficiency as shown in Eq 3 [19]:

$$\text{Solar to Vapor Conversion Efficiency} = \frac{\dot{m}\, h_{fg}}{q_{\text{Heater}}\, A}\, \tau\, \alpha \tag{3}$$

where $\dot{m}$ is the mass of collected water during 1 hour, h_{fg} is the latent heat of vaporization [20], which was fixed at 2453.5 kJ/kg for feed water at 20 °C. τ is the glass cover transmittance, which is assumed to be 0.9, and α is the absorbance of a black absorber, which is assumed to be 0.9. Previously, some researchers would multiply the optical concentration factor by the denominator terms [21–23], however, in this work, it is considered as one.

2.4. Estimation of daily water yield over a year

The daily amount of water produced during the year 2022 was estimated based on the average solar radiation during a month. Solar radiation data for the city of Dhahran in Saudi Arabia were obtained from the Prediction of Worldwide Energy Resources website of the National Aeronautics and Space Administration (NASA) [24]. Figure 5 represents the monthly average of daily global horizontal irradiance (GHI) or all sky surface shortwave downward irradiance for the months of the year. These data were used in Eq 4 [13].

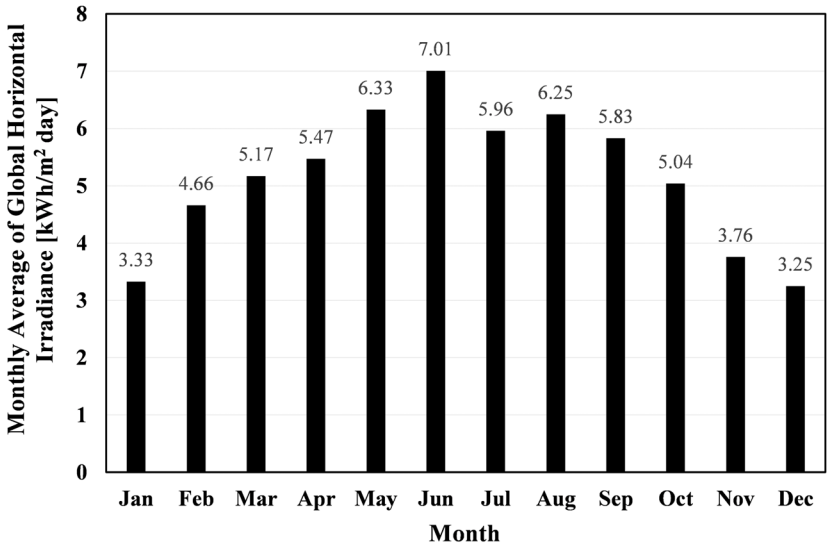

Figure 5. Monthly average of the daily global horizontal irradiance (all sky surface shortwave downward irradiance) for Dhahran, Saudi Arabia, in 2022. Data was collected from NASA's Prediction of Worldwide Energy Resources [24] website.

$$\text{Daily Water Yield}\left[\frac{\text{kg}}{\text{m}^2\text{day}}\right] = \text{GHI}\left[\frac{\text{kWh}}{\text{m}^2\ \text{day}}\right] \cdot \tau \cdot \alpha \cdot \text{Water Yield}\left[\frac{\text{kg}}{\text{kWh}}\right] \tag{4}$$

$$\text{Water Yield}\left[\frac{\text{kg}}{\text{kWh}}\right] = \frac{\dot{m}\,[\text{kg/m}^2\,\text{h}]}{q_{\text{Heater}}[\text{W/m}^2]} * 1000\,\frac{\text{W}}{\text{kW}} \tag{5}$$

where GHI is the global horizontal irradiance, τ is the glass cover transmittance, which is assumed to be 0.9, and α is the absorbance of a black absorber, which is assumed to be 0.9.

3. Results and discussion

3.1. Temperature measurements

At the beginning of the experiments, it was observed that the temperature of both the heater and the glass cover increased rapidly, but after that it began to slow down until the system reached a steady state approximately an hour after the start of the experiment, as shown in Figure 6. The figure shows the temperatures of the glass cover T_g, heater Th, last condenser T_c, feed water Tw, and ambient T_{amb}.

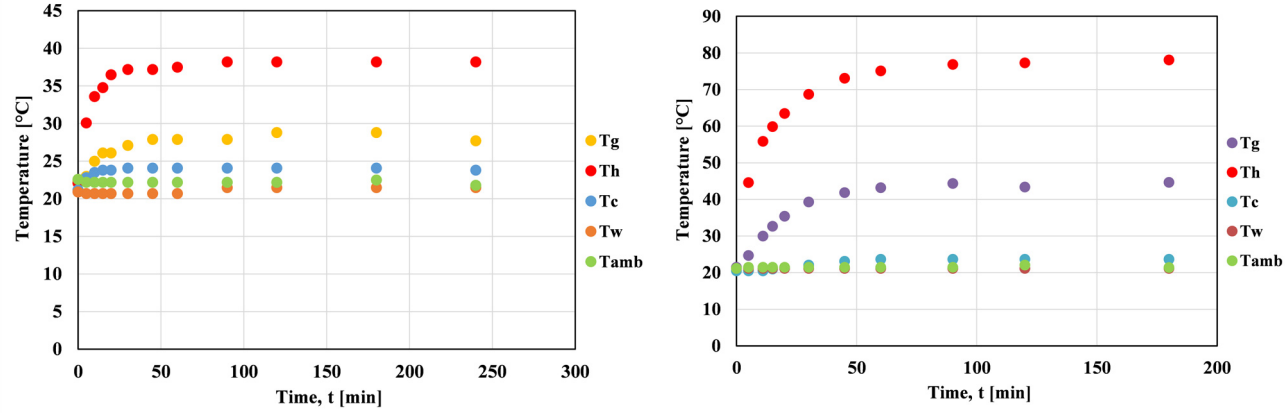

Figure 6. Temperature increment for different elements of the system with respect to time: (a) 1-Effect at 400 W/m^2; (b) 5-Effects at 1000 W/m^2.

The average temperatures for all experiments were calculated along with their standard deviations at steady state. The ambient temperature in all experiments was 21.5 ± 1.1 °C. The temperature of the feed water for all experiments was 20.6 ± 0.9 °C. The temperature of the final condenser for all experiments was 23.7 ± 2.1 °C. Temperatures of the heater and glass cover in all experiments are shown in Figure 7.

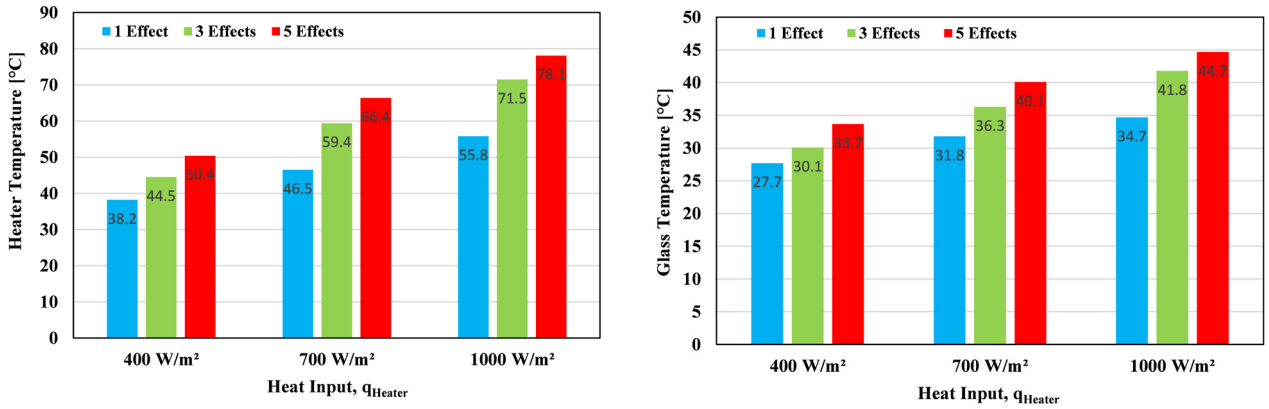

(**a**) (**b**)

Figure 7. Measured temperatures versus heat inputs at steady state for: (a) heater; (b) glass cover.

It was noticed in both Figure 7a,b that the temperatures of both the heater and the glass cover were steadily increasing. For example, when the heat input was set at 400 W/m^2, it was observed that temperatures rose with the increase of the number of effects. However, when the number of effects was fixed at 1, the temperature increased with the increase in the heat input. Nevertheless, when changing both the heat input and the number of effects, it was noted that the heater temperature at 5 effects and 700 W/m^2 exceeded itself when the heat input was 1000 W/m^2 with a one-effect configuration. In general, the high temperature of the heater was considered an advantage, as it contributed to more evaporation. Whereas, high temperature of the glass cover was considered as a disadvantage, as this indicated the presence of heat loss and poor insulation.

3.2. Salt accumulation

An experiment was conducted with 3-effects configuration and a heat input of 1000 W/m^2 for 4 hours. A photo was taken after the end of the experiment showing the first seawater collecting wick (Figure 8a) with accumulated salt over approximately one-third the area of the wick. The accumulated salt was colored in blue for the ease of view. It was observed that most of the clumped salt dissolved within less than 10 hours from the end of the experiment.

When another experiment was conducted with a 3-effects configuration and a heat input of 700 W/m^2 for 4 hours, salt accumulation was observed over an area of approximately 20% of the wick (Figure 8b). However, when the heat input was 400 W/m^2, no salt accumulation was observed. The mean value of TDS measurements of the product for all experiments was 5000 mg/L. The maximum value was 7000 mg/L, while the minimum was 3000 mg/L.

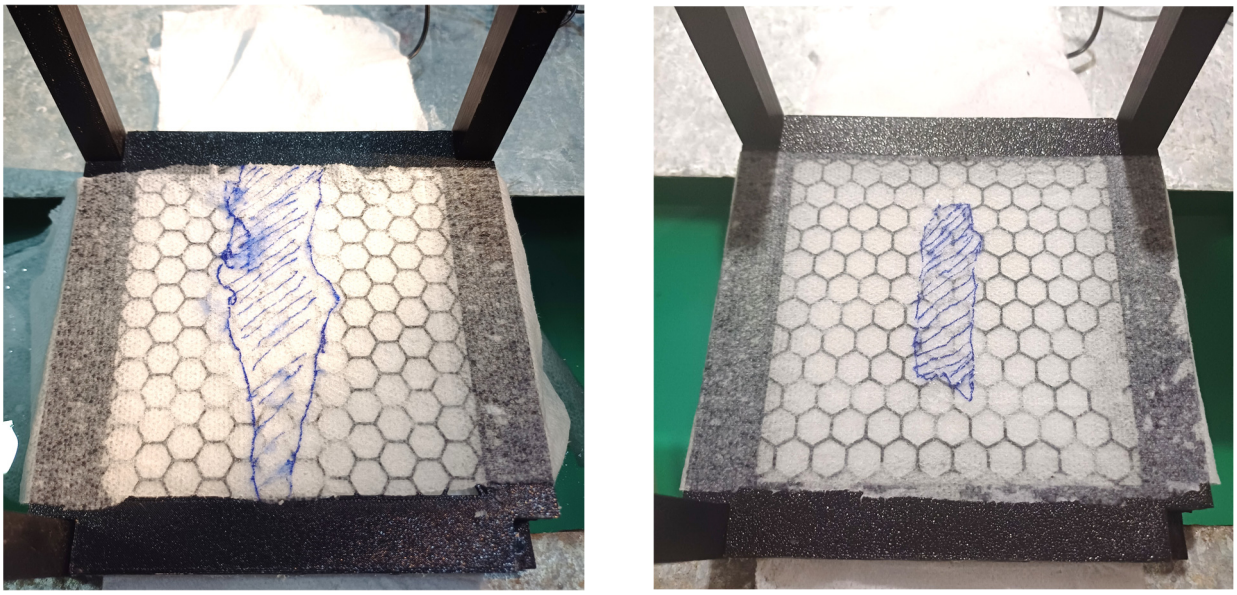

(**a**) (**b**)

Figure 8. Salt accumulation on the first seawater wick of 3-effects configuration. The snapshots were taken after 4 hours of operation at: (a) 1000 W/m^2; (b) 700 W/m^2.

3.3. Water yield, solar to vapor conversion efficiency and comparisons

Figure 9 shows the water yield per square meter per hour against the different heat inputs for the studied effects 1, 3, and 5. When focusing on the single effect configuration, one can notice a continuous increase in water yield, as it was 0.2 kg/m^2 h at 400 W/m^2 (this was the lowest value among all the experiments) and then reached 0.74 kg/m^2 h at 1000 W/m^2. The same behavior can be observed when focusing on the configuration of three effects as well as five effects. The water yield for the five-effects configuration was observed to be the highest among all the experiments at 1000 W/m^2, which reached 1.93 kg/m^2 h. However, when comparing the number of effects and the heat input for all experiments, it can be noted that the water yield of the five-effects configuration was superior to the single effect at 700 W/m^2. Likewise, it can be seen that the water yield of the three-effect configuration at 700 W/m^2 was superior to the single effect at 1000 W/m^2. Also, it can be observed that the yield of the five-effects configuration at 700 W/m^2 was close to that of three effects at 1000 W/m^2. In general, it can be concluded from Figure 9 that increasing the number of effects and increasing the heat input are directly proportional to the water yield. Some of these results could be compared with other systems. For example, Kabeel [25] conducted experiments on double-slope, concave single basin and reached a maximum water yield of 0.5 kg/m^2 h at 700 W/m^2. Also, Li et al. [26] fabricated a foldable graphene oxide film which was used as an absorber. The water yield reached 1.45 kg/m^2 at 1 kW/m^2 with four orders salinity decrement, and they outperformed the TDS value of the product in this work (4500 ppm). Ghasemi et al. [20] developed a double-layer structure consisting of a carbon foam layer supporting an exfoliated graphite layer. The maximum evaporation rate was 1.2 kg/m^2 h at 1 kW/m^2.

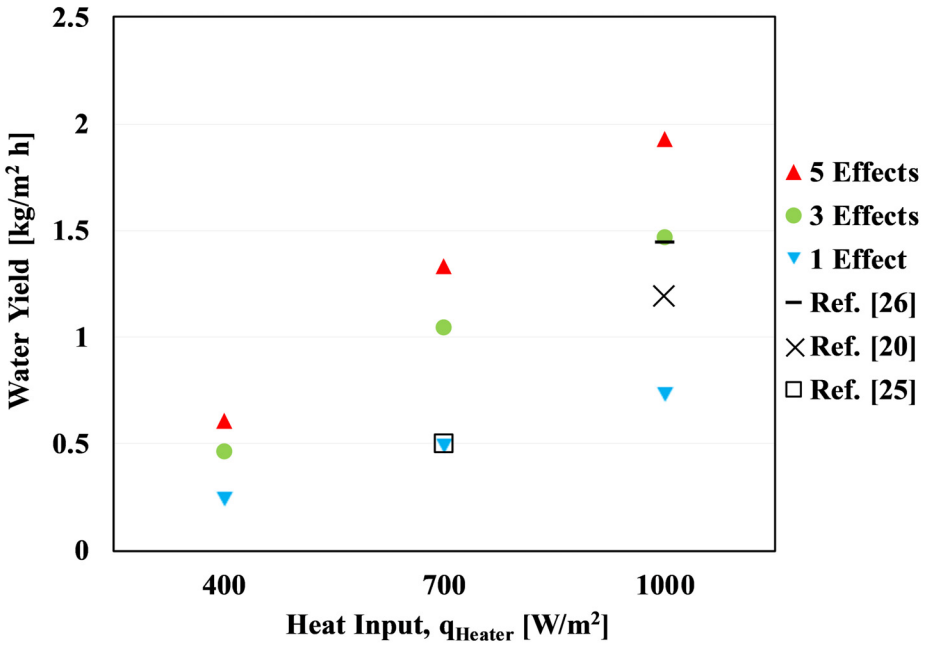

Figure 9. Water yield of horizontal multiple effects solar still versus heat input at steady state.

Regarding the solar-vapor conversion efficiency, Figure 10 shows the percentage of conversion efficiency against heat input for all studied effects. When looking at the single-effect configuration, it was noted that the conversion efficiency was the lowest at 28%, 39%, and 41% at 400, 700, and 1000 W/m^2, respectively. In the case of the three-effects configuration, the conversion efficiency was 65%, 83%, and 81% at 400, 700, and 1000 W/m^2, respectively. As for the five-effects configuration, it was the highest efficiency among the configurations, reaching 84%, 106%, and 107% at 400, 700, and 1000 W/m^2, respectively. A comparison of the results with other systems can be seen in Figure 10. The solar to vapor efficiency achieved by Ghasemi et al. [20] was 64% at 1000 W/m^2. Kabeel [25] reached 45%, while Li et al. [26] reached 80%. However, it is expected that when insulation is improved, this percentage will increase, which will raise the water yield to a value exceeding 1.47 kg/m^2 h, which was achieved by the 3-effects configuration (Figure 9). It is also important to compare the results of this work with other results regarding multiple effects distillation, whether vertical or horizontal, as shown in Table 1.

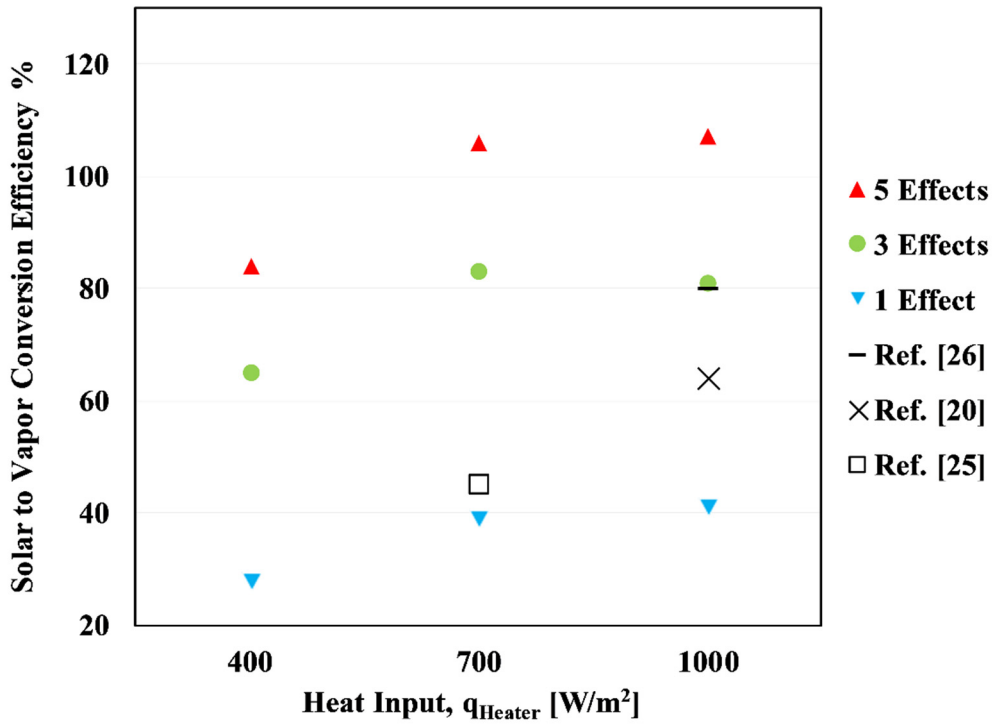

Figure 10. Conversion efficiency versus heat input for the studied effects.

Table 1. Comparison between the main findings of this paper and other previous studies.

Reference	Description	Water yield	Notes
This work	Horizontal 5-effects diffusion solar still (DSS)	Avg: 1.79 kg/kWh Max: 1.93 kg/kWh	Avg product TDS = 4500 mg/L Thermal eff. = 107%
Tanaka [10]	Vertical 6-effects DSS coupled with a flat plate reflector	2.22 kg/kWh	Tap water 13.3 kg/m^2 day @ 21.55 MJ/m^2 day
Fukuia et al. [9]	Horizontal 6-effects DSS	2.45 kg/kWh	15 kg/m^2 day @ 22 MJ/m^2 day
Tanaka and Iishi [11]	Vertical 1-effect DSS coupled with a tilted wick still	0.95 kg/kWh	4.88 kg/m^2 day @ 18.4 MJ/m^2 day Thermal eff. = 55%
Park et al. [12]	Vertical multiple effects DSS coupled with basin solar still with heated seawater	2.90 kg/kWh	18.02 kg/m^2 h @ 22.37 MJ/m^2 day
Huang et al. [14]	Vertical 6-effects cylindrical DSS with thermal concentration	2.20 kg/kWh	2.20 kg/m^2 h @ 1 kW/m^2

It can be noted that the key indexes of present DSS were not superior to some of those reported in literatures. The possible reasons could be due to low ambient temperature during the experiments, which contributes to heat loss, or poor insulation, as Zhang et al. [27] noticed that side wall insulation was a major parameter in efficiency optimization. Another source of heat loss is the extended wicks

that carry the condensed warm water out of the device. Moreover, this study was carried out without using extra elements such as reflectors or concentrators.

3.4. Estimation of daily water yield over a year

Table 2 represents a summary of all the experiments presented in the previous Figure 9, in addition to calculating the average water yield per kWh for each configuration, on which daily water yield was estimated for all months of the year.

Figure 11 shows the anticipated daily water yield and global horizontal irradiance during the months of 2022 for the city of Dhahran in Saudi Arabia. It can be noted that the maximum daily solar irradiance was in June, where it reached 7.01 kWh/m^2 day, while the lowest value was 3.25 kWh/m^2. It is become known that heat input has a significant impact on water yield, as was explained in Figure 9. Thus, it can be observed that water yields were varying for each of the three studied configurations. When we look at the month of June, we find that the water yields were 3.70, 7.85, and 10.16 kg/m^2 day for each of 1, 3, and 5 effects, respectively, and these yields were the highest of the year. However, when looking at December, it can be seen that the yields dropped to 1.71, 3.64, and 4.71 kg/m^2 day, which correspond to 1, 3, and 5 effects, respectively, and these yields were the lowest of the year.

Table 2. Summary of all experiments and calculation of average water yield per kWh.

No. of effects	Heat input [W/m^2]	Actual water yield [kg/m^2 h]	Water yield per kWh [kg/kWh]	Average water yield per kWh* [kg/kWh]
One	400	0.2	0.5	0.65
	700	0.5	0.71	
	1000	0.74	0.74	
Three	400	0.47	1.18	1.38
	700	1.05	1.50	
	1000	1.47	1.47	
Five	400	0.61	1.53	1.79
	700	1.34	1.91	
	1000	1.93	1.93	

* These values were used in the estimation of the daily water yield (kg/m^2 day).

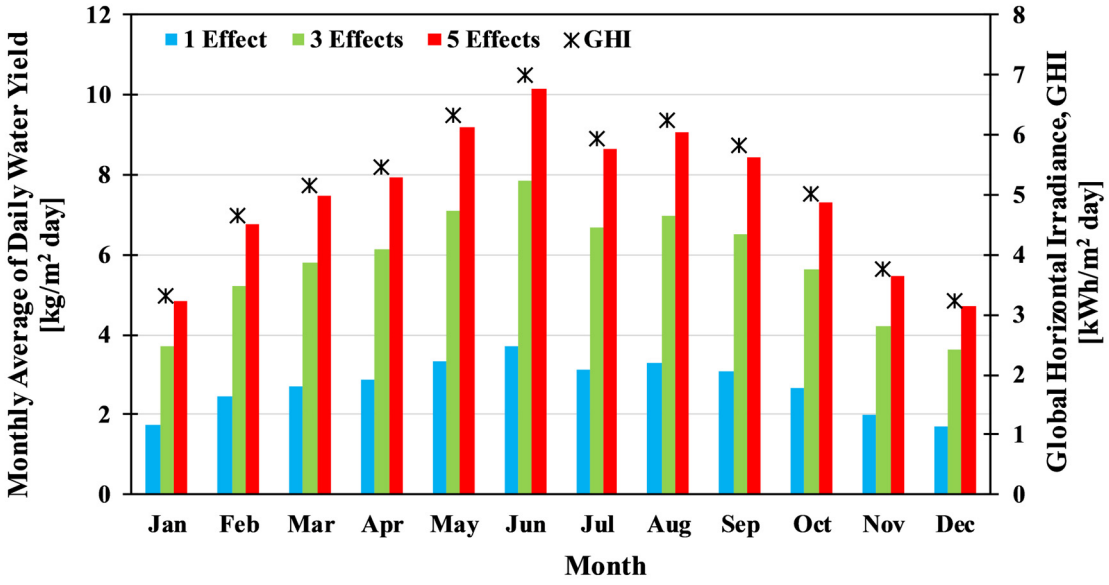

Figure 11. The estimated average daily water yield for the studied configurations during the year 2022 in Dhahran, Saudi Arabia.

4. Conclusions

In this work, a horizontal still diffusion solar device was designed and fabricated using a 3D printer. The device contained a number of layers, including: A glass cover that reduced heat dissipation, evaporators, spacers that kept the wick attached to the evaporator and allowed vapor to diffuse, then condensates. Also, some of the wicks were used to absorb seawater by capillary forces to be evaporated by the evaporator, and some of the other wicks were attached to the condenser, where the wicks were used to drive the condensed water into collectors.

In general, two parameters were studied in this research: input heat and the number of effects/stages. The range of input heat was 400, 700, 1000 W/m^2, and the range of the effects studied was 1, 3, and 5 effects. The total dissolves solids (TDS) of the seawater were 33,000 ppm. The most notable results were:

• The highest water yield was 1.93 kg/m^2 h at 5 effects and 1000 W/m^2 at steady state.

• The minimum water yield was 0.5 kg/m^2 h at single effect and 400 W/m^2 at steady state.

The average TDS of the resulting water was 4500 ppm. Although this device does not meet WHO standards for drinking water, it has shown good salinity reduction. The distillation process can be done in two stages or can be used as a pretreatment stage for other distillation techniques.

As for the average water produced per kWh, it was:

• 1.79 kg/kWh at 5 effects

• 1.38 kg/kWh at 3 effects

• 0.65 kg/kWh at single effect

The daily water yield was also estimated throughout the year in the city of Dhahran, Saudi Arabia, for all effects studied. The maximum production for five effects was 10.16 kg/m^2 day in June, while the lowest yield for the same effects was 4.71 kg/m^2 day in December.

Use of AI tools declaration

The author declares that he has not used artificial intelligence (AI) tools in the creation of this article.

Conflict of interest

The author declares no conflicts of interest.

References

1. UNICEF, WHO (2019) 1 in 3 people globally do not have access to safe drinking water, 2019. Available from: https://www.who.int/news/item/18-06-2019-1-in-3-people-globally-do-not-have-access-to-safe-drinking-water-unicef-who.
2. Likhachev DS, Li FC (2013) Large-scale water desalination methods: A review and new perspectives. *Desalination Water Treat* 51: 2836–2849. https://doi.org/10.1080/19443994.2012.750792
3. Ranjan KR, Kaushik SC (2013) Economic feasibility evaluation of solar distillation systems based on the equivalent cost of environmental degradation and high-grade energy savings. *Int J Low Carbon Technol* 11: 8–15. https://doi.org/10.1093/ijlct/ctt048
4. Younis O, Hussein AK, Attia MEH, et al. (2022) Comprehensive review on solar stills—Latest developments and overview. *Sustainability* 14: 10136. https://doi.org/10.3390/su141610136
5. Zayed ME, Kamal A, Diab MR, et al. (2023) Novel design of double slope solar distiller with prismatic absorber basin, linen wicks, and dual parallel spraying nozzles: Experimental investigation and energic-exergic-economic analyses. *Water* 15: 610. https://doi.org/10.3390/w15030610
6. Shalaby SM, El-Bialy E, El-Sebaii AA (2016) An experimental investigation of a v-corrugated absorber single-basin solar still using PCM. *Desalination* 398: 247–255. https://doi.org/10.1016/j.desal.2016.07.042
7. Manchanda H, Kumar M (2017) Performance analysis of single basin solar distillation cum drying unit with parabolic reflector. *Desalination* 416: 1–9. https://doi.org/10.1016/j.desal.2017.04.020
8. Sahota L, Tiwari GN (2017) Exergoeconomic and enviroeconomic analyses of hybrid double slope solar still loaded with nanofluids. *Energy Convers Manage* 148: 413–430. https://doi.org/10.1016/j.enconman.2017.05.068
9. Fukuia K, Nosoko T, Tanaka H, et al. (2004) A new maritime lifesaving multiple-effect solar still design. *Desalination* 160: 271–283. https://doi.org/10.1016/S0011-9164(04)90029-X
10. Tanaka H (2009) Experimental study of vertical multiple-effect diffusion solar still coupled with a flat plate reflector. *Desalination* 249: 34–40. https://doi.org/10.1016/j.desal.2008.10.022
11. Tanaka H, Iishi K (2017) Experimental study of a vertical single-effect diffusion solar still coupled with a tilted wick still. *Desalination* 402: 19–24. https://doi.org/10.1016/j.desal.2016.09.031
12. Park CD, Lim BJ, Chung KY, et al. (2016) Experimental evaluation of hybrid solar still using waste heat. *Desalination* 379: 1–9. https://doi.org/10.1016/j.desal.2015.10.004
13. Lim BJ, Yu SS, Chung KY, et al. (2018) Numerical analysis of the performance of a tiltable multi-effect solar distiller. *Desalination* 435: 23–34. https://doi.org/10.1016/j.desal.2017.12.035

14. Huang L, Jiang H, Wang Y, et al. (2020) Enhanced water yield of solar desalination by thermal concentrated multistage distiller. *Desalination* 477: 114260. https://doi.org/10.1016/j.desal.2019.114260
15. Sharon H, Reddy KS, Gorjian S (2020) Parametric investigation and year round performance of a novel passive multi-chamber vertical solar diffusion still: Energy, exergy and enviro-economic aspects. *Sol Energy* 211: 831–846. https://doi.org/10.1016/j.solener.2020.10.016
16. Xu Z, Zhang L, Zhao L, et al. (2020) Ultrahigh-efficiency desalination *via* a thermally-localized multistage solar still. *Energy Environ Sci* 13: 830–839. https://doi.org/10.1039/C9EE04122B
17. Chiavazzo E, Morciano M, Viglino F, et al. (2018) Passive solar high-yield seawater desalination by modular and low-cost distillation. *Nat Sustainability* 1: 763–772. https://doi.org/10.1038/s41893-018-0186-x
18. Çengel YA, Boles MA (2015) Thermodynamics: An engineering approach, New York, McGraw-Hill Education.
19. Zhang L, Xu Z, Zhao L, et al. (2021) Passive, high-efficiency thermally-localized solar desalination. *Energy Environ Sci* 14: 1771–1793. https://doi.org/10.1039/D0EE03991H
20. Ghasemi H, Ni G, Marconnet AM, et al. (2014) Solar steam generation by heat localization. *Nat Commun* 5: 4449. https://doi.org/10.1038/ncomms5449
21. Liu Z, Song H, Ji D, et al. (2017) Extremely cost-effective and efficient solar vapor generation under nonconcentrated illumination using thermally isolated black paper. *Glob Chall* 1: 1600003. https://doi.org/10.1002/gch2.201600003
22. Pang Y, Zhang J, Ma R, et al. (2020) Solar-thermal water evaporation: A Review. *ACS Energy Lett* 5: 437–456. https://doi.org/10.1021/acsenergylett.9b02611
23. Zhang Y, Xiong T, Nandakumar DK, et al. (2020) Structure architecting for salt-rejecting solar interfacial desalination to achieve high-performance evaporation with in situ energy generation. *Adv Sci* 7: 1903478. https://doi.org/10.1002/advs.201903478
24. National Aeronautics and Space Administration prediction of worldwide energy resources (POWER) project. Available from: https://power.larc.nasa.gov/data-access-viewer/.
25. Kabeel AE (2009) Performance of solar still with a concave wick evaporation surface. *Energy* 34: 1504–1509. https://doi.org/10.1016/j.energy.2009.06.050
26. Li X, Xu W, Tang M, et al. (2016) Graphene oxide-based efficient and scalable solar desalination under one sun with a confined 2D water path. *Proc Natl Acad Sci* 113: 13953–13958. https://doi.org/10.1073/pnas.1613031113
27. Zhang L, Xu Z, Bhatia B, et al. (2020) Modeling and performance analysis of high-efficiency thermally-localized multistage solar stills. *Appl Energy* 266: 114864. https://doi.org/10.1016/j.apenergy.2020.114864

AIMS Press